Hindawi
Wireless Communications and Mobile Computing
Volume 2023, Article ID 6785737, 9 pages
https://doi.org/10.1155/2023/6785737

Research Article

Performance Analysis of Multiple-RIS-Based NOMA Systems

Huu Q. Tran[1] **and Quoc-Tuan Vien**[2]

[1]*Industrial University of Ho Chi Minh City, Chi Minh City, Vietnam*
[2]*Middlesex University, London, UK*

Correspondence should be addressed to Huu Q. Tran; tranquyhuu@iuh.edu.vn

Received 22 July 2023; Revised 8 November 2023; Accepted 16 November 2023; Published 18 December 2023

Academic Editor: Ihsan Ali

In this paper, we present a study on a model of multirelay radio network system that utilizes reconfigurable intelligent surfaces (RISs). We investigate the use of nonorthogonal multiple access (NOMA) combined with cooperative RIS systems, using partial RIS selection (PRISs). Specifically, the RISs act as relays to forward data from the base station to the two users. The focus of this paper is to analyze the outage probabilities and throughput for the two users. Based on the results, we examine how PRISs affect the performance of the proposed NOMA scheme. The derived asymptotic expressions show that the proposed model can improve user fairness. Finally, we compare the analysis results with the simulation results and find good agreement.

1. Introduction

There are numerous challenges in fifth-generation (5G) and beyond wireless communication networks when dealing with a huge number of connected devices, demanding low latency, high-spectral efficiency, and data rates [1]. To address these issues, nonorthogonal multiple access (NOMA) technology has garnered significant attention in recent years as a promising approach for designing communication systems [2–10]. NOMA is indeed considered as a potential candidate to enhance spectral performance compared to the conventional orthogonal multiple access (OMA) techniques. In NOMA, multiple users are allowed to share the same time–frequency resources, but with different power levels and/or codebooks, enabling simultaneous transmissions [11]. For instance, compared to theconventional systems without NOMA, power allocation in NOMA prioritizes users with poorer channel conditions by allocating them more power than users with good channel conditions, thus ensuring fairness among users. In NOMA, the transmitter side utilizes signal superposition coding (SC), while the receiver side employs sequential interference cancellation (SIC). This combination allows for the separation and simultaneous transmission of signals with different power levels to multiple users over the same time and frequency resources. In SIC, the stronger user's signal is decoded and discarded first, followed by the weaker user decoding their own message [12]. This stems from the positives of NOMA in enhancing system performance. For example, the authors in [13] examined the advantages and challenges of NOMA for 5G networks. In [14], researchers are exploring the application of NOMA in the wireless downlink scenario, specifically addressing the challenges associated with multitier heterogeneous superimposed transmission. Do et al. [15] reveals that NOMA achieves superior energy efficiency (EE) compared to OMA. In [5], the concept of cooperative NOMA is explored, where the base station (BS) collaborates with users with poorer channel conditions through assisting relays. These relays play a crucial role in decoding and forwarding signals from the BS to the intended users, ensuring reliable communication over long distances or challenging propagation conditions. Cooperative NOMA leverages the relaying capabilities of assisting nodes to extend the coverage area and improve the overall system performance. By using relays, which are typically located closer to the users, the BS can overcome the limitations imposed by distance, path loss, or unfavorable channel conditions. This cooperative approach enhances the reliability and quality of communication for the users with weak channels. Regarding EE in NOMA, Yang and Yuan [10] investigates simultaneous wireless information and power transfer (SWIPT) techniques. SWIPT is a concept where wireless devices can simultaneously receive information and harvest energy from the received signals. By integrating

power transfer functionality into NOMA systems, SWIPT aims to enhance EE and enable self-sustainability for the wireless devices. SWIPT allows NOMA-enabled devices to harvest energy from the signals transmitted by the BS while concurrently decoding the information contained in those signals. This energy harvesting (EH) capability can potentially reduce the reliance on traditional power sources and improve the EE of NOMA-based systems. The research in [10] likely explores various aspects of SWIPT in NOMA, such as power control strategies, resource allocation techniques, and tradeoffs between EH and information decoding. These investigations aim to maximize the EE of NOMA systems and explore the feasibility of integrating wireless power transfer into NOMA-enabled networks. To gain a comprehensive understanding of the findings and methodologies of Yue et al. [5] and Yang and Yuan [10], it is advisable to refer to the respective research papers for more in-depth information. To enhance EE in NOMA, researchers have investigated SWIPT [10]. In the mentioned approach, stochastic geometry is employed to take into account the spatial positions of users and radio EH at relays, which assists in forwarding signals to distant users. Stochastic geometry is a mathematical framework that models the random spatial distribution of wireless devices in a network. By incorporating stochastic geometry, the researchers consider the spatial locations of users and the availability of relays with radio EH capabilities. This enables a more realistic representation of the network environment and allows for the analysis of performance metrics, such as coverage, interference, and energy efficiency. The use of relays with EH capabilities is particularly beneficial for forwarding signals to distant users. These relays can harvest energy from received signals and utilize it to amplify and forward the signals to users who are farther away from the BS or have weaker channel conditions. This cooperative NOMA approach, with the aid of relays, enhances the overall performance of the system by extending coverage and improving the reliability of communication. Regarding the study in [4], Tran et al. have examined the performance of systems aiming to achieve the capacity of the broadcasting channel using a single-antenna downlink NOMA strategy. In downlink NOMA, the BS broadcasts signals to multiple users simultaneously in the same time–frequency resource. The authors likely investigate the capacity limits and achievable performance in such a NOMA system with a single antenna at the BS. The study in [4] likely includes analyses, mathematical modeling, and performance evaluations of the proposed single-antenna downlink NOMA strategy. The authors may consider factors such as power allocation, decoding strategies, and interference management to maximize the system capacity and explore the potential benefits of NOMA in achieving the capacity of the broadcasting channel. For detailed insights, it is recommended to refer to the specific research paper [4] for a comprehensive understanding of the authors' methodologies, findings, and contributions in the context of achieving channel capacity using single-antenna downlink NOMA. Recently, with the introduction of reconfigurable intelligent surfaces (RIS) [16], there have been proposals for systems that combine NOMA networks with RIS reconfigurable smart surfaces. The combination between NOMA networks and RIS has been demonstrated to be highly compatible and complementary, and also highlights that RIS is viewed as an important technology for achieving a smart radio environment for sixth-generation wireless communication network technology [17]. RIS can act as a passive reflector that collects wireless signals from a transmitter and directs them toward a receiver, potentially enhancing the overall signal strength and quality. An RIS is a planar surface comprising a large number of tiny reflecting elements, known as metasurfaces or melements (N metasurface melements), that can be dynamically controlled to manipulate electromagnetic waves passing through them. These metasurfaces are typically composed of subwavelength resonant structures that can alter the phase, amplitude, and polarization of the incident waves. By carefully adjusting the reflection properties of each melement, an RIS can steer waves in a desired direction, amplify or attenuate them, or even create new beams [1]. Overall, the use of RISs has the potential to revolutionize wireless communication by enabling high-speed and reliable connectivity in challenging environments such as crowded urban areas, indoor spaces, and remote locations. Researchers have been motivated by the potential advantages of RISs and have explored their integration into various key technologies. These include deep learning [18, 19], wireless energy transfer [20], and NOMA [21]. Over the past 2 years, significant attention has been given to the performance analysis and system optimization of wireless communication systems aided by intelligent reflecting surfaces (IRSs), particularly under Rayleigh [22, 23] and Rician fading channels [24–26]. In [24], asymptotic expressions were derived for the upper bound on channel capacity and the outage probability (OP), considering Rician fading over the IRS links and modeling the direct-link channel as Rayleigh fading. Liu and Zhang [27] investigated a 5G-based IoT system that leverages the 5G spectrum to transmit both 5G and IoT information simultaneously. The proposed system utilizes the 5G network to transmit voice and video information from internet of things (IoT) nodes, while the IoT network is utilized to forward sensing data. In [28], a novel approach was studied for power-constrained IoT networks, which utilizes NOMA and is assisted by an RIS for uplink transmissions. Meanwhile, Chu et al. [29] investigated a multi-IRS-assisted multicluster wireless-powered IoT network, where IoT devices use the fractional nonlinear EH model to harvest energy for their information transmission with the aid of multiple IRSs.

In this paper, we consider a relay radio network system that utilizes RISs to forward data from a BS to two destination nodes (D_1 and D_2). Specifically, we investigate the use of NOMA combined with cooperative RIS systems, where partial RIS selection (PRIS) is employed.

The paper presents several key contributions of our work, which are summarized as follows:

(i) We propose a multiple-RIS approach in NOMA systems, where the BS transmits signals to two NOMA users via reflected paths. The channel model considered for this approach is in line with the 5G standard, making the use of multiple-RIS-based NOMA systems more suitable and practical.

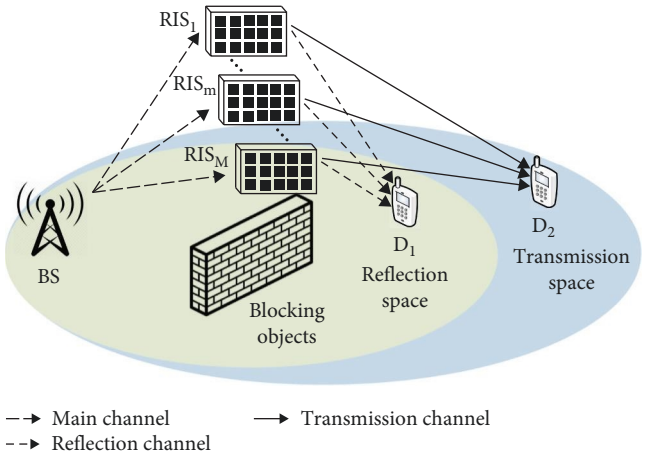

FIGURE 1: System model.

(ii) We derive the expressions for the outage probability (OP) and throughput at two users, D_1 and D_2, in the multiple-RIS-based NOMA systems over Rayleigh fading channels.

(iii) The closed-form expressions are presented in terms of the OP, enabling a comprehensive system throughput analysis. To validate the derived expressions, we conducted Monte Carlo simulations using MATLAB on a personal computer.

The remainder of this article is organized as follows: Section 2 shows the system model and channel characteristics. In Section 3, we analyze the outage performance and system throughput of NOMA schemes considering both perfect SIC and imperfect SIC. In Section 4, we have included an in-depth discussion of energy efficiency. Section 5 presents numerical results and Monte Carlo simulations to validate the theoretical analysis. Finally, we conclude the article in Section 6.

2. System Model and Channel Characteristics

Figure 1 illustrates the wireless communication system that we consider, which consists of a BS equipped with one transmit antenna, two users (D_1 and D_2), each equipped with one receive antenna. It is assumed that there are obstacles from BS to D_1 and from BS to D_2. So, BS cannot transmit a signal directly to D_1 and D_2. Each RIS is composed of N_m reflecting components. However, for the sake of simplicity, we will assume that the M RIS devices are the same, i.e., $N = N_1 = N_2 = \ldots = N_M$. Three prominent RIS protocols, including ES, temporal switching (TS), and mode switching (MS), have been developed for simultaneous transmitting and reflecting RIS systems [30]. It is important to note that power-splitting circuits are necessary for the ES protocol, and energy leakage is unavoidable. Additionally, mode-switching circuits are required for each element in the TS protocol. Consequently, the MS protocol is regarded as having the simplest implementation [30]. According to Liu et al. [31], we make the following assumptions: the RISs contain N components, N_R for reflection and N_T for transmission, with $N_R + N_T = N$. In practice, in the context of IRS, a controller is often employed to dynamically adjust the phases of the reflecting elements [32]. This enables the IRS to optimize its beamforming capabilities and enhance the performance of the wireless communication system. Similar to the study of Basar et al. [1], it is assumed that full knowledge of the CSI is available. The communication process begins with the BS transmitting the signal to the m-th RIS $(m = 1, 2, \ldots, M)$, which then reflects the signal passively to D_1 and D_2. To that purpose, the m-th RIS (denoted by RIS_m for simplicity) optimizes the phase reflection coefficient to maximize the received signal-to-interference-plus-noise ratio (SINR) at D_1 and D_2, hence boosting the communication system's end-to-end quality. We assume that the channels experience independent Rayleigh fading.

In particular, we assume that the distant user (D_2) with low channel gains is the weak user and the close user (D_1) with excellent channel gains is the strong user. To improve D_2's communication quality, a power imbalance is introduced by setting $a_2 > a_1$, and both power coefficients are required to satisfy the constraint $a_1 + a_2 = 1$, as described in [2–4]. Here, a_1 and a_2 denote the power distribution coefficients for user D_1 and user D_2, respectively. By allocating more power to user D_2, the system can enhance the signal quality at D_2 and improve its overall performance. The mixed signal $(a_1 + a_2)$ is transmitted from the BS to the mth RIS (RIS_m), where x_1 is the unit signal required by D_1 and x_2 is the unit signal required by D_2. The signals are then passively reflected by RIS_m to D_1 and D_2. Thus, the signal received by close user D_1 and far user D_2 may be expressed as follows:

$$\tilde{y}_{D_1}^m = \left[\sum_{q_r=1}^{N_R} h_{mq_r} g_{mq_r,1} e^{j\phi_{mq_r}^R}\right](\sqrt{P_S a_1}x_1 + \sqrt{P_S a_2}x_2) + \tilde{\omega}_{D_1}^m, \tag{1}$$

$$\tilde{y}_{D_2}^m = \left[\sum_{q_t=1}^{N_T} h_{mq_t} g_{mq_t,2} e^{j\phi_{mq_t}^T}\right](\sqrt{P_S a_1}x_1 + \sqrt{P_S a_2}x_2) + \tilde{\omega}_{D_2}^m. \tag{2}$$

Here, $g_{mq_r,1}$ and $g_{mq_t,2}$ represent the channel gains for the $\mathrm{RIS_m} - \mathrm{D_1}$ and $\mathrm{RIS_m} - \mathrm{D_2}$ links, respectively. h_{mq_r} and h_{mq_t} represent the channel gains for the $\mathrm{BS} - \mathrm{RIS_m}$ with N_R for reflection and N_T for transmission. In Equations (1) and (2), $\phi_{mq_r}^R$ and $\phi_{mq_t}^T$ denote the adjustable phase produced by the q_rth and q_tth reflecting elements of $\mathrm{RIS_m}$, where q_r ranges from 1 to N_R and q_t ranges from 1 to N_T. We set $h_{mq_r} = d_{SR_m}^{-\delta/2}\alpha_{mq_r}e^{-j\theta_{mq_r}}$, $h_{mq_t} = d_{SR_m}^{-\delta/2}\alpha_{mq_t}e^{-j\theta_{mq_t}}$, $g_{mq_r,1} = d_{R_mD_1}^{-\delta/2}\beta_{mq_r,1}e^{-j\varepsilon_{mq_r,1}}$, and $g_{mq_t,2} = d_{R_mD_2}^{-\delta/2}\beta_{mq_t,2}e^{-j\varepsilon_{mq_t,2}}$. We assume that the distance from the BS to the M RIS devices is equal, and that the distance from the M RIS devices to D_1 is also equal, with the distance from the M RIS devices to D_2 being the same. The distances for $\mathrm{BS} - \mathrm{RIS_m}$, $\mathrm{RIS_m} - \mathrm{D_1}$, and $\mathrm{RIS_m} - \mathrm{D_2}$ links are denoted as d_{SR_m}, $d_{R_mD_1}$, and $d_{R_mD_2}$, respectively. Additionally, the RISs do not suffer from phase

errors. δ represents the path loss coefficient, while α_{mq_r}, α_{mq_t}, $\beta_{mq_r,1}$, and $\beta_{mq_t,2}$ denote the channel amplitudes. The phases of the fading channels are denoted as θ_{mq_r}, θ_{mq_t}, $\varepsilon_{mq_r,1}$, and $\varepsilon_{mq_t,2}$. Additionally, $\bar{\omega}_{D_1} \sim \mathcal{CN}(0, \omega_{D_1}^2)$ and $\bar{\omega}_{D_2} \sim \mathcal{CN}(0, \omega_{D_2}^2)$ represent the additive white Gaussian noise (AWGN) samples. Similarly to the study by Basar et al. [1], we assume that RIS_m has perfect knowledge of the h_{mq_r}, h_{mq_t}, $g_{mq_r,1}$, and $g_{mq_t,2}$ channel phases. According to Yue et al. [5], SIC technology can be employed in NOMA systems to decipher the signals of distinct users. The weak user, D_1, has poor channel gains and can only decode its own signal. However, it lacks the capability to extract D_2's signal from the mixed signals. As a result, D_1 suffers from additional interference from D_2, and the instantaneous SINR for D_1 can be represented as follows:

$$\bar{\gamma}_{1,x_2}^m = \frac{a_2 P_S \left| \sum_{q_r=1}^{N_R} \alpha_{mq_r} \beta_{mq_r,1} e^{j\left(\phi_{mq_r}^R - \theta_{mq_r} - \varepsilon_{mq_r,1}\right)} \right|^2}{a_1 P_S \left| \sum_{q_r=1}^{N_R} \alpha_{mq_r} \beta_{mq_r,1} e^{j\left(\phi_{mq_r}^R - \theta_{mq_r} - \varepsilon_{mq_r,1}\right)} \right|^2 + \zeta_1 \omega_{D_1}^2}, \tag{3}$$

where $\zeta_1 = d_{SR_m}^{\delta} d_{R_m D_1}^{\delta}$. We presume that the RIS is aware of the legal far users' CSI. The phase $\phi_{mq_r}^R$ generated by the q_rth reflecting component of the m-th RIS in RIS-aided wireless communication systems is adjusted to optimize the received signal strength at the receiver. The value of $\phi_{mq_r}^R$ is determined so that the phase error $\phi_{mq_r}^R - \theta_{mq_r} - \varepsilon_{mq_r,1}$ equals zero based on the structure of the RISs and the perfect channel state information known by the RIS controller. In other words, we have $\phi_{mq_r}^R - \theta_{mq_r} - \varepsilon_{mq_r,1} = 0, \forall q_r, \forall m$. In both mathematical analysis and measurement studies of RIS-aided wireless communication systems, this assumption was frequently employed in the literatures [1, 6–8]. Therefore, we may employ phase shifting to optimize $\bar{\gamma}_{1,x_2}^m$ when $\phi_{mq}^1 = \theta_{mq} + \varepsilon_{mq,1}$. As a result, the maximized $\bar{\gamma}_{1,x_2}^m$ can be expressed as follows:

$$\begin{aligned} \bar{\gamma}_{1,x_2}^m &= \frac{a_2 P_S \left| \sum_{q_r=1}^{N_R} \alpha_{mq_r} \beta_{mq_r,1} \right|^2}{a_1 P_S \left| \sum_{q_r=1}^{N_R} \alpha_{mq_r} \beta_{mq_r,1} \right|^2 + \zeta_1 \omega_{D_1}^2} \\ &= \frac{a_2 \rho_S A^2}{a_1 \rho_S A^2 + \zeta_1}, \end{aligned} \tag{4}$$

where $A \triangleq \left| \sum_{q_r=1}^{N_R} \alpha_{mq_r} \beta_{mq_r,1} \right|$, we assume that $\rho_S = \frac{P_S}{\omega_{D_1}^2} = \frac{P_S}{\omega_{D_2}^2}$ represents the average transmit signal-to-noise ratio (SNR) (dB). It should be noted that x_1 and x_2 are normalized unity power signals, i.e., $\mathbb{E}\{x_1^2\} = \mathbb{E}\{x_2^2\} = 1$ where $\mathbb{E}\{\cdot\}$ denotes the expectation operator. In the case of incomplete SIC, the received SINR at D_1 for detecting its own message x_1 is given by:

$$\bar{\gamma}_{1,x_1}^m = \frac{a_1 \rho_S A^2}{\xi a_2 \rho_S A^2 + \zeta_1}. \tag{5}$$

Here, $\xi, 0 \le \xi \le 1$ depicts the efficiency of SIC for x_2 at the D_1. The parameter ξ has two specific values, 0 and 1, that correspond to two cases: perfect SIC (where $\xi = 0$) and no SIC ($\xi = 1$). We assume that $\phi_{mq_t}^T = \theta_{mq_t} + \varepsilon_{mq_t,2}$ for the q_t-th reflecting elements of the m-th RIS can be optimized [9]. Consequently, the received signal and SINR at user D_2 are formulated as follows:

$$\begin{aligned} \bar{\gamma}_2^m &= \frac{a_2 P_S \left| \sum_{q_t=1}^{N_T} \alpha_{mq_t} \beta_{mq_t,2} e^{j\left(\phi_{mq_t}^T - \theta_{mq_t} - \varepsilon_{mq_t,2}\right)} \right|^2}{a_1 P_S \left| \sum_{q_t=1}^{N_T} \alpha_{mq_t} \beta_{mq_t,2} e^{j\left(\phi_{mq_t}^T - \theta_{mq_t} - \varepsilon_{mq_t,2}\right)} \right|^2 + \zeta_2 \omega_{D_2}^2} \\ &= \frac{a_2 P_S \left| \sum_{q_t=1}^{N_T} \alpha_{mq_t} \beta_{mq_t,2} \right|^2}{a_1 P_S \left| \sum_{q_t=1}^{N_T} \alpha_{mq_t} \beta_{mq_t,2} \right|^2 + \zeta_2 \omega_{D_2}^2} \\ &= \frac{a_2 \rho_S B^2}{a_1 \rho_S B^2 + \zeta_2}, \end{aligned} \tag{6}$$

where $B \triangleq \left| \sum_{q_t=1}^{N_T} \alpha_{mq_t} \beta_{mq_t,2} \right|$ and $\zeta_2 = d_{SR_m}^{\delta} d_{R_m D_2}^{\delta}$.

3. Performance Analysis

In this part, we examine the OP and throughput of the system under consideration. Throughout the analytical derivations, we assume that one of the M RISs is chosen to aid communication. Specifically, the appropriate RIS is selected to optimize the received signal at the destination. Therefore, the RIS's selection principle can be represented as follows:

$$m_1^* = \arg \max_{m_1 \in \{1,2,\ldots,M\}} \bar{\gamma}_1^m, \tag{7}$$

$$m_2^* = \arg \max_{m_2 \in \{1,2,\ldots,M\}} \bar{\gamma}_2^m, \tag{8}$$

where $\bar{\gamma}_1^m = \min\left(\frac{\bar{\gamma}_{1,x_1}^m}{\varepsilon_1}, \frac{\bar{\gamma}_{1,x_2}^m}{\varepsilon_2}\right)$ in which $\varepsilon_2 = 2^{R_2} - 1$ with R_2 is the target rate at D_2 for detecting x_2, and $\varepsilon_1 = 2^{R_1} - 1$ with R_1 is the target rate at D_1 for detecting x_1. Based on order statistics theory, the cumulative distribution function (CDF) of $\bar{\gamma}_1^{m_1^*}$ and $\bar{\gamma}_2^{m_2^*}$ in Equations (7) and (8) can be written as follows:

$$F_{\bar{\gamma}_1^{m_1^*}}(x) = \left[F_{\bar{\gamma}_1^m}(x) \right]^M, \tag{9}$$

$$F_{\bar{\gamma}_2^{m_2^*}}(x) = \left[F_{\bar{\gamma}_2^m}(x) \right]^M. \tag{10}$$

This results in the probability density function (PDF) shown below as follows:

$$f_{\bar{\gamma}_1^{m_1^*}}(x) = M f_{\bar{\gamma}_1^m}(x) \left[F_{\bar{\gamma}_1^m}(x) \right]^{M-1}, \tag{11}$$

$$f_{\bar{\gamma}_2^{m_2^*}}(x) = M f_{\bar{\gamma}_2^m}(x) \left[F_{\bar{\gamma}_{2,x_2}^m}(x) \right]^{M-1}. \tag{12}$$

3.1. Outage Probability Analysis. The complementing events of D_1's outage may be explained using the NOMA protocol as follows: D_1 can detect both x_2 and its own message x_1. Based on the above explanation, the outage probability at D_1 can be written as follows:

$$
\begin{aligned}
P_1 &= \Pr\left(\bar{\gamma}_1^{m_1^*} < 1\right) \\
&= \Pr\left(\min\left(\frac{\bar{\gamma}_{1,x_1}^{m_1^*}}{\varepsilon_1}, \frac{\bar{\gamma}_{1,x_2}^{m_1^*}}{\varepsilon_2}\right) < 1\right) \\
&= 1 - \Pr\left(\bar{\gamma}_{1,x_2}^{m_1^*} > \varepsilon_2, \bar{\gamma}_{1,x_1}^{m_1^*} > \varepsilon_1\right) \\
&= 1 - \Pr\left(A^2 > \frac{\varepsilon_2\zeta_1}{\rho_S(a_2 - \varepsilon_2 a_1)}, A^2 > \frac{\varepsilon_1\zeta_1}{\rho_S(a_1 - \varepsilon_1\xi a_2)}\right) \\
&= \begin{cases} 1 - \Pr(A^2 > \Phi_{\max}) & , \text{if } a_2 > \varepsilon_2 a_1 \\ 1 & , \text{if } a_2 < \varepsilon_2 a_1, \end{cases}
\end{aligned} \tag{13}
$$

where $\Phi_{\max} = \max(\frac{\varepsilon_2\zeta_1}{\rho_S(a_2 - \varepsilon_2 a_1)}, \frac{\varepsilon_1\zeta_1}{\rho_S(a_1 - \varepsilon_1\xi a_2)})$. The outage probability at D_2 can be interpreted as follows: user D_2 is unable to detect its own message x_2. The outage probability of D_2 is expressed as follows:

$$
\begin{aligned}
P_2 &= 1 - \Pr\left(\bar{\gamma}_2^{m_2^*} > \varepsilon_2\right) \\
&= \begin{cases} 1 - \Pr\left(B^2 > \dfrac{\varepsilon_2\zeta_2}{\rho_S(a_2 - \varepsilon_2 a_1)}\right) & , \text{if } a_2 > \varepsilon_2 a_1 \\ 1 & , \text{if } a_2 < \varepsilon_2 a_1. \end{cases}
\end{aligned} \tag{14}
$$

We assume a multiple RIS-aided system setup where the RIS with the highest instantaneous SNR is chosen to aid communication. The exact expression for the outage probability is derived using both the noncentral chi-square (NCCS) distribution and the K_G distribution, as shown below.

3.1.1. NCCS Distribution. Using the approach provided in [10, Equation (6)], the PDF of Z, where $Z \in \{A^2, B^2\}$, $h \in \{R, T\}$, can be expressed as follows:

$$
f_Z(x) = \frac{1}{2\sigma_h^2}\left(\frac{x}{\lambda_h}\right)^{-\frac{1}{4}} e^{-\frac{x+\lambda_h}{2\sigma_h^2}} I_{-\frac{1}{2}}\left(\frac{\sqrt{x\lambda_h}}{\sigma_h^2}\right). \tag{15}
$$

Here, $I_a(\cdot)$ represents the first-order modified Bessel function [11], λ_h is set to $(\frac{N_h\pi}{4})^2$, and σ_h^2 is equal to $N_h(1 - \frac{\pi^2}{16})$. Therefore, the CDF of Z can be expressed as follows [12, Equation (9)]:

$$
F_Z(x) = 1 - Q_{\frac{1}{2}}\left(\frac{\sqrt{\lambda_h}}{\sigma_h}, \frac{\sqrt{x}}{\sigma_h}\right). \tag{16}
$$

Here, $Q_v(r, u)$ denotes the Marcum Q-function as defined in [13]. Thus, the system's OP for two users can be expressed as follows:

$$
P_1 = \left[1 - Q_{\frac{1}{2}}\left(\frac{\sqrt{\lambda_R}}{\sigma_R}, \frac{\sqrt{\Phi_{\max}}}{\sigma_R}\right)\right]^M, \tag{17}
$$

$$
P_2 = \left[1 - Q_{\frac{1}{2}}\left(\frac{\sqrt{\lambda_T}}{\sigma_T}, \frac{\sqrt{\varepsilon_2\zeta_2}}{\sigma_T\sqrt{\rho_S(a_2 - \varepsilon_2 a_1)}}\right)\right]^M. \tag{18}
$$

3.1.2. K_G Distribution. Many publications typically use the central limit theorem to obtain the NCCS distribution for analyzing the performance of RIS-aided systems. However, the NCCS distribution is only accurate for high values of N, as stated in [14]. To provide a comparison, we also present an analysis using the K_G distribution proposed in [14]. The PDF of Z can be expressed as follows [14]:

$$
f_Z(x) = \frac{2\Xi^{k+m}}{\Gamma(k)\Gamma(m)} x^{\frac{k+m-2}{2}} K_{k-m}\left(2\Xi\sqrt{x}\right). \tag{19}
$$

The CDF of Z can be calculated using the following formula, where k and m are shaping parameters, $\Gamma(\cdot)$ is the Gamma function, $K_a(\cdot)$ is the modified Bessel function of the second type with zero order, Ω is the mean power, and $\Xi = \sqrt{km/\Omega}$ represents the correlation coefficient. Here, k and m are the shaping parameters, $\Gamma(\cdot)$ represents the Gamma function, $K_a(\cdot)$ is the modified Bessel function of the second type with zero order, Ω denotes the mean power, and $\Xi = \sqrt{km/\Omega}$ represents the correlation coefficient. As a result, the CDF of Z may be calculated as follows:

$$
F_Z(x) = \frac{1}{\Gamma(k)\Gamma(m)} G_{1,3}^{2,1}\left(\Xi^2 x \middle| \begin{matrix} 1 \\ k, m, 0 \end{matrix}\right). \tag{20}
$$

Here, $G_{p,q}^{f,n}(\cdot)$ refers to the Meijer G-function, as defined in [11]. The closed-form expressions for the outage probabilities at D_1 and D_2 are given by:

$$
P_1 = \left[\frac{1}{\Gamma(k)\Gamma(m)} G_{1,3}^{2,1}\left(\Xi^2\Phi_{\max} \middle| \begin{matrix} 1 \\ k, m, 0 \end{matrix}\right)\right]^M, \tag{21}
$$

$$
P_2 = \left[\frac{1}{\Gamma(k)\Gamma(m)} G_{1,3}^{2,1}\left(\frac{\Xi^2\varepsilon_2\zeta_2}{\rho_S(a_2 - \varepsilon_2 a_1)} \middle| \begin{matrix} 1 \\ k, m, 0 \end{matrix}\right)\right]^M. \tag{22}
$$

3.2. Throughput Analysis. In this section, we further study a measure of throughput in delay-limited transmission mode based on outage performance. This throughput represents the system's capacity when a certain data rate is required. We can obtain the throughput at these key nodes, as shown in Equation (23):

Table 1: Main system parameters.

Monte Carlo simulations	10^7 Iterations
The targeted data rate for users	$R_1 = R_2 = 1$ (b/s/Hz)
Number of RISs	$M = 3$
Total reflecting elements	$N = 32$
Bandwidth	BW = 10 (MHz)
Noise figure	NF = 10 (dBm)
Thermal noise power density	$N_0 = -174$ (dBm/Hz)
The distance from BS to RIS_m	$d_{SR_m} = 60$ (m)
The distance from RIS_m to D_1	$d_{R_m D_1} = 100$ (m)
The distance from RIS_m to D_2	$d_{R_m D_2} = 150$ (m)
The path loss exponent	$\alpha = 2$

$$\tau_i = (1 - P_i)R_i \quad , i \in \{1, 2\}. \tag{23}$$

4. Energy Efficiency

To attain higher throughput in delay-constrained transmission, additional investigations are needed to explore the EE of multiple-RIS-enabled NOMA systems. As indicated in [5, Equation (52)], the expression for the EE coefficient is given by

$$\eta_{EE} = \frac{\text{Total data rate}}{\text{Total energy consumption}}. \tag{24}$$

Thus, the EE values for the multiple-RIS-based NOMA systems may be rewritten as follows:

$$\eta_P^{EE} = \frac{\tau_1 + \tau_2}{TMP_S}. \tag{25}$$

In this context, the variable T represents the duration of the transmission process, covering the entire communication, whereas M stands for the number of RIS employed.

5. Numerical Results

In this section, we assessed the performance of the derived theoretical expression and produced numerical results to validate the analytical expression. The main parameters are listed in Table 1. Additionally, the equivalent noise power at D_1 and D_2 was calculated as $\omega_{D_1}^2 = \omega_{D_2}^2 = N_0 + 10\log(\text{BW}) + \text{NF}$ (dBm) in [15]. Our code's technological contribution is the use of symbolic calculations in MATLAB, which allowed us to achieve very accurate results.

In Figure 2, we compare the OP of the RIS-NOMA system with a scenario where M RISs are equipped with N reflecting components and imperfect SIC for D_1. Here, $M = 3, 5$, $N_R = N_T = 8, 16$, $a_1 = 0.1$, $a_2 = 0.9$, and $R_1 = R_2 = 1$ (b/s/Hz). In Section 3.1, we utilize Equations (17), (18), (21), and (22) to plot analytical curves, denoted as "Ana." in Figure 2 and subsequent images. Simultaneously, we obtain simulation results using Equations (13) and (14), represented as "Sim." It is evident that the OP for $M = 3$ and $N_R = N_T = 8$ (the planned RIS-NOMA system) is significantly higher than that for $M = 5$ and $N_R = N_T = 16$. Specifically, to achieve an outage probability of 10^{-2} at D_1 and D_2 in the RISs scenario, the transmission power of BS is set to -10, -5, and 0 dBm, respectively. Meanwhile, in the case of $M = 3$ and $N_R = N_T = 8$, the power levels are 5, 10, and 15 dBm. In simpler terms, to achieve the same OP target of 10^{-8} by using five RISs, each with sixteen reflecting components, the transmission power of the BS can be reduced by -5, 0, and 10 dBm, respectively, compared to the scenario with three RISs. Additionally, among the NOMA coefficients, D_2 exhibits the best OP, while D_1 has the lowest. Furthermore, it is possible to derive a lower OP of 10^{-15} using the analytical formulas. Unfortunately, achieving this result through Monte Carlo simulation is not feasible.

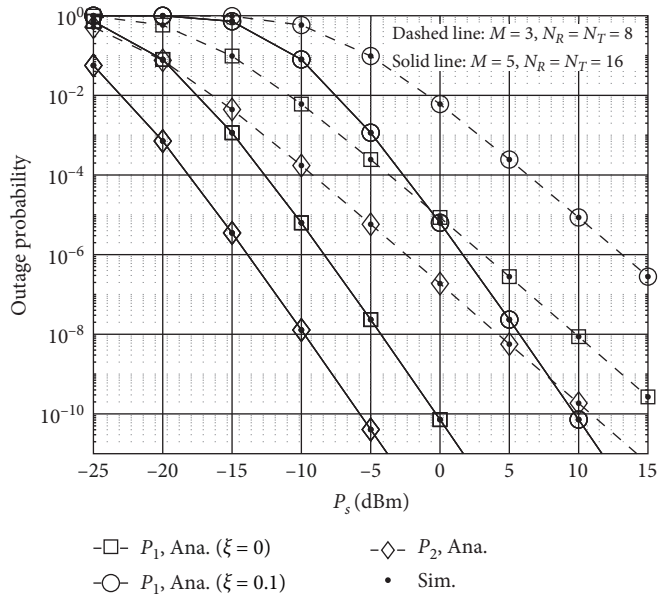

Figure 2: The outage probability for different combinations pairs of (M, N_R, N_T).

Figure 3 depicts the ideal OP of users D_1, D_2 at various locations of a_2. These findings can be explained by the fact that power allocation factors a_1 and a_2 contribute to the variance in SINR as well as the associated outage probability, with $a_2 = 0.65$ demonstrating the best OP for D_1. Additionally, these findings show that changing the number of RISs has a high effect on the outage likelihood, as evidenced by the two users in the observed region. It is intuitive that high-transmit power at the BS would result in greater outage performance.

Figure 4 depicts an analysis of the OP versus targeted data rates $R_1 = R_2$ with residual interference of $\xi = 0.0316$ and transmit power $P_S = -15$ and $P_S = 10$ (dBm). Once again, we can observe the effect of imperfect SIC and transmit power as throughput increases. Lower $R_1 = R_2$ rates produce the best outage performance. It is worth noting that Figures 2–4 all illustrate the significance of using multiple RISs and phase shifts for each RIS in relation to the outage likelihood for downlink RIS-NOMA systems.

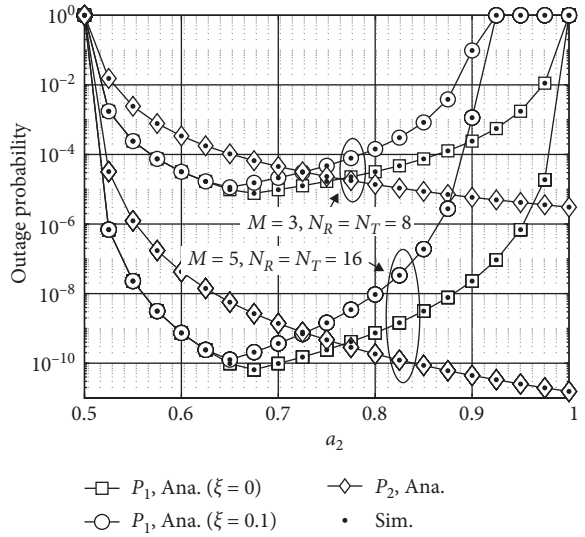

FIGURE 3: The outage probability at D_1 and D_2 versus a_2 with $P_S = -5$ (dBm).

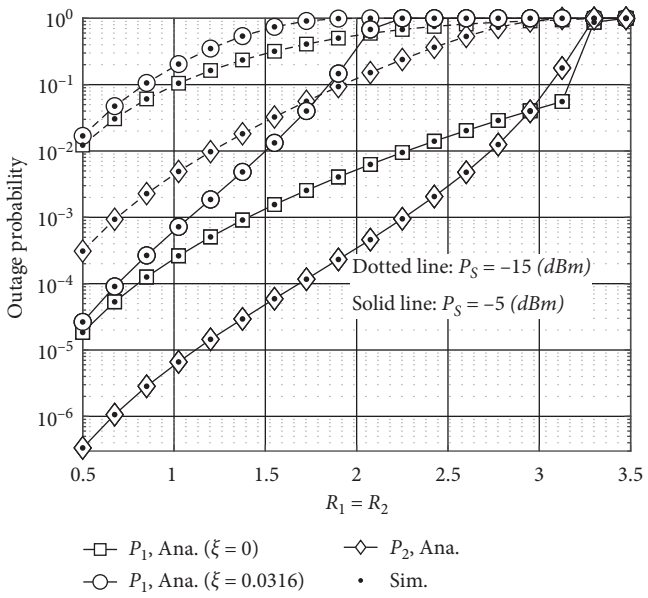

FIGURE 4: The outage probability at D_1 and D_2 versus a_2 with $M = 3$ and $N_R = N_T = 8$.

Figure 5 displays the OP of RIS-NOMA and relay-NOMA as a function of P_S in dBm for $M = 3$ and $N_R = N_T = 16$. From the graph, it becomes evident that the OP of the RIS-NOMA system is significantly lower than that of the relay-NOMA system as P_S increases gradually. This figure underscores the superiority of the system supported by RIS in comparison to the relay-NOMA system, as discussed in detail in [33].

Figure 6 demonstrates that the throughput reaches its maximum at the desired rates in the high-transmission power zone. Due to its better outage performance, as shown in the previous figures, the throughput of user D_2 can approach the maximum value sooner than in other

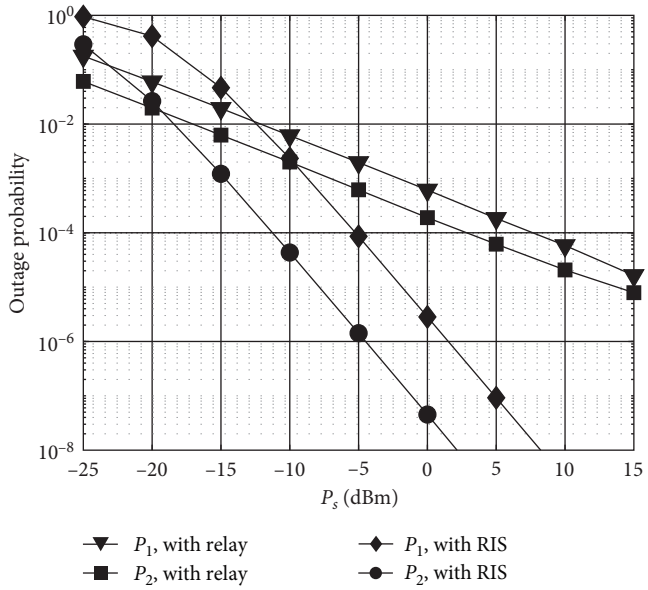

FIGURE 5: The outage probability comparison between RIS-assisted NOMA systems and relay-assisted NOMA systems, with $M = 3$ and $N_R = N_T = 16$.

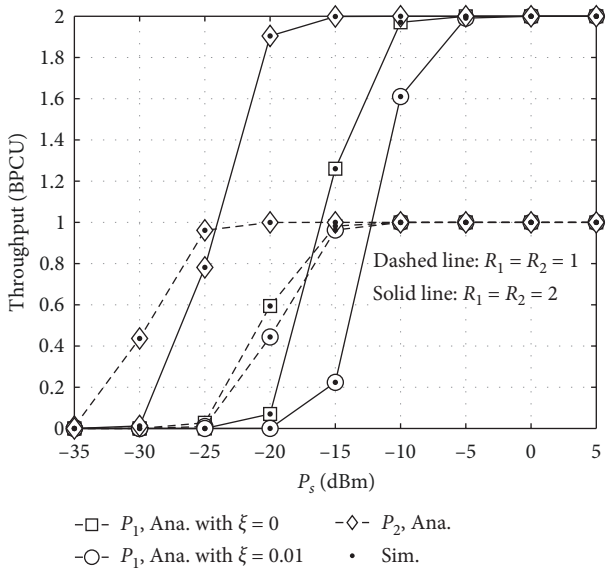

FIGURE 6: Throughput in delay-limited transmission mode versus SNR, with $a_1 = 0.05$, $a_2 = 0.95$, $d_{SR_m} = 60$ m, $d_{R_m D_1} = 100$ m, $d_{R_m D_2} = 150$ m, $\delta = 2$, $M = 5$, and $N_R = N_T = 16$.

scenarios. These findings are consistent with the equations computed in Equation (23).

In NOMA systems, as depicted in Figure 7, the system's EE is plotted against P_S at the source, considering a mode that allows for delay-limited transmission for user relaying. When $M = 5$, the system's EE in the delay-limited transmission mode is lower than when $M = 3$. It becomes evident that $M = 3$ yields the highest value for the system's EE when $M = 5$. However, it is worth noting that the EE of such systems is constrained in areas with high-transmit SNR. This limitation is

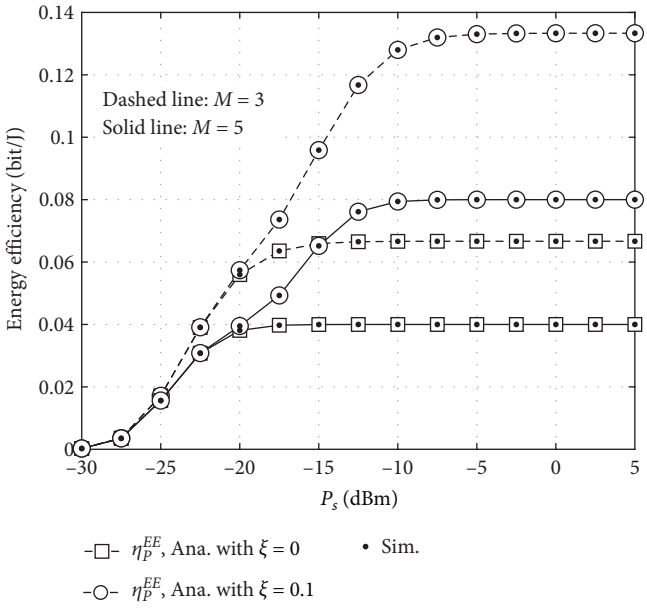

FIGURE 7: System energy efficiency transmits SNR at the source. The parameters are as follows: $a_1 = 0.05$, $a_2 = 0.95$, $d_{SR_m} = 60$ m, $d_{R_m D_1} = 100$ m, $d_{R_m D_2} = 150$ m, $\delta = 2$, $R_1 = R_2 = 2$, $N_R = N_T = 16$, $T = 1$, and $P_S = 10$ W.

due to the outage probability associated with the delay-limited transmission mode, which impacts the system's energy efficiency. In high-SNR regions, both outage probability performances reach saturation.

6. Conclusion

In this paper, we have investigated the OP and the throughput of NOMA schemes for a multirelay radio network system that utilizes RIS. We have provided numerical derivations of NOMA protocols in two cases: perfect SIC and imperfect SIC. The analytical evaluations of NOMA protocols based on perfect SIC at average SNR are always superior to NOMA with imperfect SIC. Additionally, the outage performance of the User 1 is consistently higher than that of User 2. The results show that when the values of P_S are lower, the outage performances are higher. Conversely, when the value of P_S is higher, the OPs are lower. Moreover, lower $R_1 = R_2$ rates result in the best outage performance. Furthermore, the analytical expressions show that imperfect SIC considerably impacts the OP and the system throughput. The higher the system throughput, the larger $R_1 = R_2$. Numerical results confirm that our derivative analysis results are consistent with the Monte Carlo simulation results for all possible system parameters. For future work, we can enhance the performance of the multirelay system by developing the system that utilizes multiple antennas at two users, D_1 and D_2, while also considering the possibility of establishing a direct connection between the BS and the users.

Data Availability

The data used to support the findings of this study are included in the paper.

Conflicts of Interest

The authors declare that they have no conflicts of interest.

Authors' Contributions

Huu Q. Tran contributed in the conceptualization, methodology, software, formal analysis, and investigation. Huu Q. Tran contributed in the data curation and writing-original draft preparation. Huu Q. Tran and Quoc-Tuan Vien contributed in the validation and resources. Huu Q. Tran and Quoc-Tuan Vien contributed in the writingreviewing and editing.

Acknowledgments

Huu Q. Tran acknowledges the support of time and facilities from the Faculty of Electronics Technology, Industrial University of Ho Chi Minh City for this study. This study was self-funded by the authors.

References

[1] E. Basar, M. Di Renzo, J. de Rosny, M. Debbah, M.-S. Alouini, and R. Zhang, "Wireless communications through reconfigurable intelligent surfaces," *IEEE Access*, vol. 7, pp. 116753–116773, 2019.

[2] H. Q. Tran, T.-T. Nguyen, C. V. Phan, and Q.-T. Vien, "Power-splitting relaying protocol for wireless energy harvesting and information processing in NOMA systems," *IET Communications*, vol. 13, no. 14, pp. 2132–2140, 2019.

[3] H. Q. Tran, C. V. Phan, and Q.-T. Vien, "Power splitting versus time switching based cooperative relaying protocols for SWIPT in NOMA systems," *Physical Communication*, vol. 41, Article ID 101098, 2020.

[4] H. Q. Tran, C. V. Phan, and Q.-T. Vien, "Performance analysis of power-splitting relaying protocol in SWIPT based cooperative NOMA systems," *EURASIP Journal on Wireless Communications and Networking*, vol. 2021, Article ID 110, 2021.

[5] X. Yue, Y. Liu, S. Kang, A. Nallanathan, and Z. Ding, "Exploiting full/half-duplex user relaying in NOMA systems," *IEEE Transactions on Communications*, vol. 66, no. 2, pp. 560–575, 2018.

[6] S. Atapattu, R. Fan, P. Dharmawansa, G. Wang, J. S. Evans, and T. A. Tsiftsis, "Reconfigurable intelligent surface assisted two-way communications: performance analysis and optimization," *IEEE Transactions on Communications*, vol. 68, no. 10, pp. 6552–6567, 2020.

[7] E. Björnson, Ö. Özdogan, and E. G. Larsson, "Intelligent reflecting surface versus decode-and-forward: how large surfaces are needed to beat relaying?" *IEEE Wireless Communications Letters*, vol. 9, no. 2, pp. 244–248, 2020.

[8] A. Bansal, K. Singh, and C.-P. Li, "Analysis of hierarchical rate splitting for intelligent reflecting surfaces-aided downlink multiuser MISO communications," *IEEE Open Journal of the Communications Society*, vol. 2, pp. 785–798, 2021.

[9] B. C. Nguyen, L. T. Dung, T. M. Hoang, N. V. Vinh, and G. T. Luu, "On performance of multi-RIS assisted multi-user nonorthogonal multiple access system over Nakagami-*m* fading channels," *Computer Communications*, vol. 197, pp. 294–305, 2023.

[10] L. Yang and Y. Yuan, "Secrecy outage probability analysis for RIS-assisted NOMA systems," *Electronics Letters*, vol. 56, no. 23, pp. 1254–1256, 2020.

[11] I. S. Gradshteyn and I. M. Ryzhik, *Table of Integrals, Series and Products*, Academic Press, San Diego, CA, 7th edition, 2007.

[12] L. Yang, Y. Yang, D. B. da Costa, and I. Trigui, "Outage probability and capacity scaling law of multiple RIS-aided networks," *IEEE Wireless Communications Letters*, vol. 10, no. 2, pp. 256–260, 2021.

[13] V. M. Kapinas, S. K. Mihos, and G. K. Karagiannidis, "On the monotonicity of the generalized Marcum and Nuttall *Q*-Functions," *IEEE Transactions on Information Theory*, vol. 55, no. 8, pp. 3701–3710, 2009.

[14] L. Yang, F. Meng, Q. Wu, D. B. da Costa, and M. Alouini, "Accurate closed-form approximations to channel distributions of RIS-aided wireless systems," *IEEE Wireless Communications Letters*, vol. 9, no. 11, pp. 1985–1989, 2020.

[15] T. N. Do, G. Kaddoum, T. L. Nguyen, D. B. da Costa, and Z. J. Haas, "Multi-RIS-aided wireless systems: statistical characterization and performance analysis," *IEEE Transactions on Communications*, vol. 69, no. 12, pp. 8641–8658, 2021.

[16] Q. Wu and R. Zhang, "Towards smart and reconfigurable environment: intelligent reflecting surface aided wireless network," *IEEE Communications Magazine*, vol. 58, no. 1, pp. 106–112, 2020.

[17] M. Di Renzo, A. Zappone, M. Debbah et al., "Smart radio environments empowered by reconfigurable intelligent surfaces: how it works, state of research, and the road ahead," *IEEE Journal on Selected Areas in Communications*, vol. 38, no. 11, pp. 2450–2525, 2020.

[18] S. Zhang, S. Zhang, F. Gao, J. Ma, and O. A. Dobre, "Deep learning-based RIS channel extrapolation with element-grouping," *IEEE Wireless Communications Letters*, vol. 10, no. 12, pp. 2644–2648, 2021.

[19] C. Huang, R. Mo, and C. Yuen, "Reconfigurable intelligent surface assisted multiuser MISO systems exploiting deep reinforcement learning," *IEEE Journal on Selected Areas in Communications*, vol. 38, no. 8, pp. 1839–1850, 2020.

[20] E. Shi, J. Zhang, S. Chen et al., "Wireless energy transfer in RIS-aided cell-free massive MIMO systems: opportunities and challenges," *IEEE Communications Magazine*, vol. 60, no. 3, pp. 26–32, 2022.

[21] X. Mu, Y. Liu, L. Guo, J. Lin, and N. Al-Dhahir, "Exploiting intelligent reflecting surfaces in NOMA networks: joint beamforming optimization," *IEEE Transactions on Wireless Communications*, vol. 19, no. 10, pp. 6884–6898, 2020.

[22] Y. Zhang, J. Zhang, M. D. Renzo, H. Xiao, and B. Ai, "Performance analysis of RIS-aided systems with practical phase shift and amplitude response," *IEEE Transactions on Vehicular Technology*, vol. 70, no. 5, pp. 4501–4511, 2021.

[23] A. A. Boulogeorgos and A. Alexiou, "Performance analysis of reconfigurable intelligent surface-assisted wireless systems and comparison with relaying," *IEEE Access*, vol. 8, pp. 94463–94483, 2020.

[24] Q. Tao, J. Wang, and C. Zhong, "Performance analysis of intelligent reflecting surface aided communication systems," *IEEE Communications Letters*, vol. 24, no. 11, pp. 2464–2468, 2020.

[25] I. Yildirim, A. Uyrus, and E. Basar, "Modeling and analysis of reconfigurable intelligent surfaces for indoor and outdoor applications in future wireless networks," *IEEE Transactions on Communications*, vol. 69, no. 2, pp. 1290–1301, 2021.

[26] A. M. Salhab and M. H. Samuh, "Accurate performance analysis of reconfigurable intelligent surfaces over rician fading channels," *IEEE Wireless Communications Letters*, vol. 10, no. 5, pp. 1051–1055, 2021.

[27] X. Liu and X. Zhang, "Rate and energy efficiency improvements for 5G-based IoT with simultaneous transfer," *IEEE Internet of Things Journal*, vol. 6, no. 4, pp. 5971–5980, 2019.

[28] M. AlaaEldin, E. Alsusa, K. G. Seddik, and M. Al-Jarrah, "Optimizing IRS-assisted uplink NOMA system for power constrained IoT networks," in *2022 IEEE 96th Vehicular Technology Conference (VTC2022-Fall)*, pp. 1–6, London, United Kingdom, 2022.

[29] Z. Chu, P. Xiao, D. Mi, W. Hao, Y. Xiao, and L.-L. Yang, "Multi-IRS assisted multi-cluster wireless powered IoT networks," *IEEE Transactions on Wireless Communications*, vol. 22, no. 7, pp. 4712–4728, 2023.

[30] Y. Liu, X. Mu, J. Xu et al., "STAR: simultaneous transmission and reflection for 360° coverage by intelligent surfaces," *IEEE Wireless Commun*, vol. 28, no. 6, pp. 102–109, 2021.

[31] H. Liu, G. Li, X. Li, Y. Liu, G. Huang, and Z. Ding, "Effective capacity analysis of STAR-RIS-assisted NOMA networks," *IEEE Wireless Communications Letters*, vol. 11, no. 9, pp. 1930–1934, 2022.

[32] N. Van Vinh and P. Van Tri, "Performance assessment of millimeter-wave NOMA system with intelligent reflecting surface," *IEEE Access*, vol. 10, pp. 66143–66152, 2022.

[33] T. M. Hoang, N. T. Tan, N. H. Hoang, and P. T. Hiep, "Performance analysis of decode-and-forward partial relay selection in NOMA systems with RF energy harvesting," *Wireless Networks*, vol. 25, no. 8, pp. 4585–4595, 2019.